JOURNAL OF AIRCRAFT
Vol. 36, No. 6, November–December 1999

Parametric Study of the Behavior of Graphite/Epoxy Panels with Stiffener Terminations

Dawn C. Jegley*
NASA Langley Research Center, Hampton, Virginia 23681-2199

The results of a parametric study examining six types of stiffener terminations for stiffened graphite/epoxy panels are presented. Stiffener blades are terminated by attaching to another blade, by tapering the stiffener height, by tapering the stiffener thickness, or by a combination of these methods. Stiffener flanges are also terminated abruptly or by tapering their thickness. Flange length is also varied. Both thin-skin panels and thick-skin panels are considered. Panels were analyzed with a nonlinear finite element analysis code to determine panel response and failure modes. Midplane axial and shear strains, surface strains, interlaminar strains, and failure predictions for the panels are discussed. These results indicate that the mechanism initiating failure is dependent on the stringer configuration of the panel. Interlaminar stresses and bending must be considered to predict the failure of thin-skin panels, and interlaminar stress, in-plane shear strains, and axial strains must be considered to predict the failure of thick-skin panels.

Introduction

ONE of NASA's goals is to reduce the cost of air travel by 50% in the next 20 years. To achieve this cost reduction, NASA is assisting in the development of the technology needed for future low-cost, lightweight composite structures for commercial transport aircraft. As part of this effort, a stitched graphite/epoxy material system has been identified to have the potential for reducing both the weight and cost of commercial transport aircraft wing structure. By stitching through the thickness of a dry graphite preform prior to adding epoxy resin, the labor associated with wing cover panel fabrication and assembly can be significantly reduced. By stitching through the thickness of prestacked skin material and then stitching together stringers, intercostals, and spar caps with the skin material, the need for mechanical fasteners is almost eliminated. This manufacturing approach reduces part count and, therefore, the cost of the structure. Stiffener terminations are an integral part of wing cover panels used in commercial transport aircraft. Terminating stiffeners induces stress concentrations and large local stress gradients that must be considered during the wing cover panel design. When stiffeners are bonded and stitched with no additional fasteners, stiffener terminations can become one of the most critical detail features of the cover panel. Therefore, structural response and failure modes associated with stiffener terminations must be understood before stitched cover panels can be used on commercial aircraft.

To examine the behavior of stitched composite panels with stiffener terminations, an analytical parametric study was conducted by varying stiffener geometry, and the results of this study are presented. Stiffener geometry variations are in the form of gradual reductions or tapers in stiffener thickness, stiffener height, or both. The analytical study also includes thick-skin and thin-skin panels. The finite element models and nonlinear analysis approach validated previously and described in Ref. 1 has been used for the present study. These panels were cut from the undamaged region of a previously tested 12-ft-long, stitched graphite/epoxy wing box, described in Ref. 2. This wing box was fabricated by the McDonnell Douglas Aerospace Company as part of the NASA Advanced Composites Technology Program, and was loaded to failure at the NASA Langley Research Center. Panels with five other types of stiffener configurations, but with the same global dimensions and properties as the test panels, were analyzed in the present study to examine differences in strains, predicted failure locations, and predicted failure modes.

Panel Descriptions

Two similar undamaged panels were cut from the tested McDonnell Douglas wing box. The panels were fabricated from Hercules, Inc., AS4/3501-6 graphite/epoxy materials that were stitched together using E. I. DuPont de Nemours, Inc., Kevlar® thread. The composite skin and stiffeners were fabricated from layers of the graphite material forms that were prekitted into nine-ply stacks. Each nine-ply stack had a $[45/-45/0_2/90/0_2/-45/45]_T$ laminate stacking sequence and was approximately 0.058 in. thick. Several nine-ply stacks of the prekitted material were used to build up the desired thickness at each location. The composite wing box was fabricated using the resin film infusion process that is described in Ref. 3.

The stringers and intercostals are blade stiffeners that are approximately 2.3 in. tall. All stringer blades in the panels are nominally 0.46 in. thick (eight stacks) with a 1.12-in.-wide flange on either side of the web. All intercostal blades are nominally 0.116 in. thick (two stacks) with a 1.1-in.-wide flange on either side of the web. Intercostals are perpendicular to the stringers. A graphite/epoxy rib was bolted to each intercostal in the original wing box. This rib was cut to match the height of the intercostal in the test panels rather than risk damaging the intercostal by removing the bolts. Because of last minute concerns that the stringer-termination or runout region would fail prematurely in the wing box test, a row of bolts was added to each flange of a terminating stringer to prevent the stringer flange from separating from the skin. However, the wing box was originally designed with no mechanical fasteners at the stringer runouts, and any further studies would not include these fasteners.

The geometry of the test panels is shown in Fig. 1. The stringer blade is eight-stacks thick at the thicker end and two-stacks thick at the termination point or thinner end. Stacks are terminated on both sides of the blade at 3-in. intervals. Stringer flanges are always half the thickness of the blade. The stringer blade terminates at the intercostal by folding out into tabs that are placed against the intercostal blade, as shown in Fig. 1. The test panels are 15.25 in. long and 10.0 in. wide with the intercostal located 2 in. from one end of the panel.

Received 6 February 1999; presented as Paper 99-1407 at the AIAA/ASME/ASC/AHS 40th Structures, Structural Dynamics, and Materials Conference, St. Louis, MO, 12–15 April 1999; revision received 15 May 1999; accepted for publication 19 May 1999.

*Senior Aerospace Engineer, Structural Mechanics Branch, Structures and Materials Competency, Mail Stop 190. Senior Member AIAA.

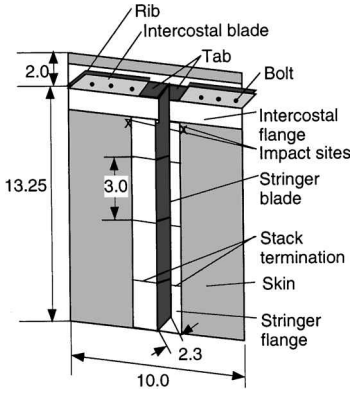

Fig. 1 Geometry of test panel, length dimensions in inches.

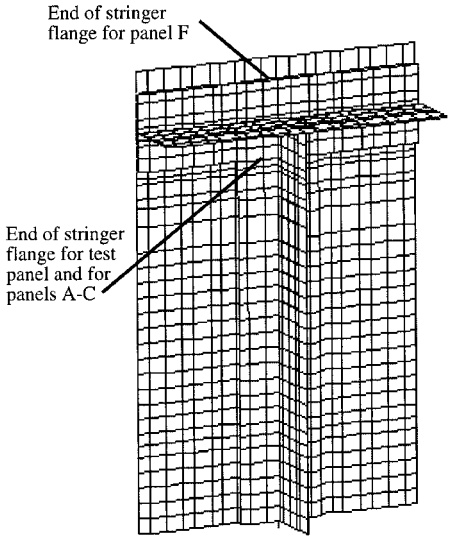

Fig. 2 Finite element model of test panel and panels with a constant-height blade (configurations A, B, C, and F).

The loaded edges of the panels were potted in an epoxy compound that was 1 in. deep to simulate clamped end conditions and to prevent end failures. These loaded ends were ground flat and parallel to each other prior to testing.

Loading and Instrumentation

The test panels were loaded in axial compression. Knife edge supports were used on the unloaded edges of the panels to minimize out-of-plane motion of the skin. No support was provided for the intercostal or intercostal flange. The panels were instrumented with strain gauges and direct current displacement transducers were used to monitor end-shortening and out-of-plane displacements. Panels were loaded to failure at a load rate of approximately 10,000 lb/min.

Analysis

A geometrically nonlinear analysis of the test panels was conducted with the finite element code STAGS.[4] The model used to analyze the panels is shown in Fig. 2. This model includes 1325, four-node quadrilateral elements and 10,019 degrees of freedom. The model of the test panels includes the stack terminations in the blade and flanges. Material properties for the stitched material used in the analysis are shown in Table 1. The intercostal and rib were included in the model; however, fasteners through the skin were not included in the analysis. Stringer and intercostal flanges were modeled separately from the skin so that stresses between the flanges and the skin could be evaluated. The link between the flange and the skin was provided by rigid links joining each skin and flange node pair. The lengths of these links were required to be constant throughout loading. All displacements and rotations of each flange node were required to be the same as the displacements and rotations of its adjacent skin node. Initial node positions were selected

Table 1 Material properties

Property	Value
Longitudinal stiffness	8.17×10^6 psi
Transverse stiffness	4.46×10^6 psi
Shear stiffness	2.35×10^6 psi
Poisson's ratio	0.458
Allowable axial strain (no damage)	0.0093 in./in.
Allowable axial strain (with damage)	0.0053 in./in.
Allowable shear strain	0.0126 in./in.

Table 2 Stringer termination configurations considered, thin and thick skin

Configuration	Blade height	Blade thickness	Intercostal attachment	Extended flange
A	Constant	Tapered	Yes	No
B	Constant	Tapered	No	No
C	Constant	Constant	Yes	No
D	Tapered	Tapered	No	No
E	Tapered	Constant	No	No
F	Constant	Tapered	Yes	Yes

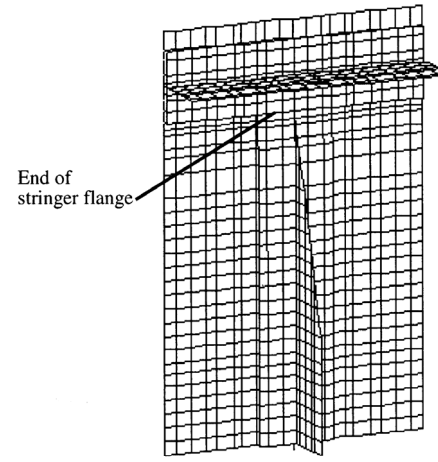

Fig. 3 Finite element model of panel with a tapered-height blade (configurations D and E).

to allow the flange nodes to be accurately offset from the skin nodes (based on skin and flange thickness at each location).

In addition to the test panel configuration, five other configurations of stringer terminations were analyzed. The test panel configuration contained a constant-height, tapered-thickness stringer that was bonded to the intercostal. This configuration is configuration A. The second configuration, configuration B, contained a constant-height, tapered-thickness stringer that was terminated abruptly at the intercostal and was not connected to it. The third configuration, configuration C, contained a constant-height, constant-thickness stringer that was connected to the intercostal. The model for configuration C is the same as the model for the test panel except for the blade and flange thicknesses. The fourth configuration, configuration D, contained a tapered-height, tapered-thickness stringer. The model of this configuration is shown in Fig. 3. The fifth configuration, configuration E, contained a tapered-height, constant-thickness stringer, for which the model is the same as for configuration D except for blade and flange thicknesses. The sixth configuration is the same as configuration A except that the flange of the stringer is continued underneath the intercostal flange and terminates at the opposite edge of the intercostal flange, as shown in Fig. 2. All of these configurations are listed in Table 2.

All panels contained an eight-stack-thick blade away from the intercostal and a two-stack-thick intercostal. Thin panels with a five-stack skin, like the test panels, and thick panels with a 10-stack skin were examined. Simple support boundary conditions along the entire unloaded edges, including the intercostal flanges, were used for the parametric study. All thin-skin panels have the same far-field

cross-sectional area, and the variation in weight among the six thin-skin panels is approximately 12% of the weight of the heaviest thin-skin panel. A wing cover panel would typically have a rib spacing in the vicinity of 30 in. and numerous stringers. The difference in weight of this design detail would have less than a 2% effect on the weight of wing cover panel overall and a much smaller percent of the weight in the entire wing box. Load-carrying capability and manufacturing concerns would have more influence on the selection of the runout configuration than runout weight in most cases. Similarly, all thick-skin panels have the same far-field cross-sectional area, and the variation in weight among the six thick-skin panels is less than 10% in these panels. In a wing cover panel the difference in weight of this design detail has less effect thick-skin wing cover panel than on a thin-skin wing cover panel.

Results

Experimental and analytical results are presented in this section for the test panel. For graphical comparisons between experimental and analytical results, experimental results are shown as solid lines and analytical results are shown as dashed lines. Analytical results are then presented for panels with six types of stringer terminations for thin-skin panels and then for the same six types of stringer terminations for thick-skin panels. The effect of impact damage to thin- and thick-skin panels is also discussed.

Test Panels

Two test panels were loaded to failure in axial compression. One panel was not damaged prior to loading, and one panel was subjected to severe impact damage prior to compressive loading. The axial surface strains in the skin of the undamaged panel at a distance 4.75 in. away from the intercostal are shown in Fig. 4. Results from back-to-back strain gauges agree well with each other, indicating that little bending occurs away from the intercostal. The axial strains in the skin at the edge of the intercostal flange are shown in Fig. 5. Experimental and analytical results indicate that bending behavior occurs in the region of the intercostal flange. Additional strain and displacement results are presented in Ref. 1 for both test panels and analysis. Analytical and experimental results are in good agreement.

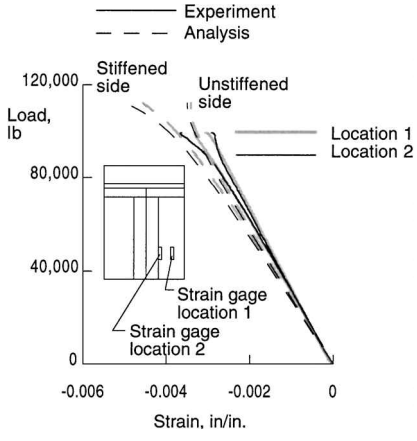

Fig. 4 Axial far-field strain in the skin of test panel.

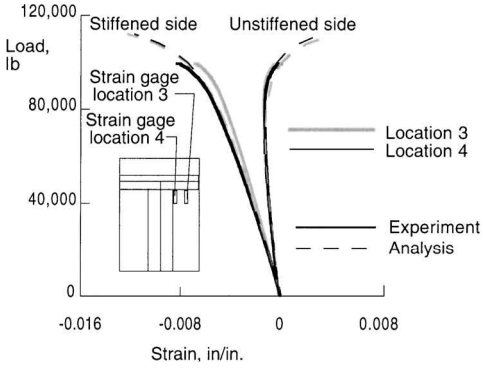

Fig. 5 Axial strain in skin near the intercostal flanges for test panel.

Analysis indicates that the maximum compressive axial surface strain occurs in the intercostal flange near the intercostal, but the maximum axial strain at the laminate midplane occurs in the stringer flange near the intercostal. Based on an allowable axial strain value at the laminate midplane of 0.0093 in./in. for undamaged structure, failure should not occur due to axial strain for a load less than 108,500 lb. Lateral strains were small enough to have little effect on failure. However, the in-plane shear strain in the intercostal flange is predicted to exceed the shear strain allowable of 0.0126 in./in. for loads greater than 91,200 lb. In-plane shear strain in the intercostal flange causes or contributes to failure of the panel because the panel failed at 99,200 lb. The effect of the fasteners through the skin was neglected for two reasons. First, ideally the fasteners would have not been included in the panel, and the strength of the stitches would have been the only mechanism available to suppress delamination. Second, the fasteners may have prevented catastrophic failure of the test panel, but test data indicate that after delamination began, the panel retained little ability to support additional load. Post-test evaluation of the panel indicated that there were delaminations and broken stitches between the skin and stringer flange, but no evidence of failure at the fasteners.

The predicted interlaminar stresses, normalized by material failure stresses, can be combined to evaluate interlaminar stresses between the stringer flanges and the skin (see Ref. 5). The assumed interlaminar tensile normal stress at failure, $F_z = 5{,}900$ lb/in.^{2}, and the assumed interlaminar shear stress at failure, $F_s = 13{,}500$ lb/in.^{2}, are used to obtain an interlaminar failure parameter. A normalized interlaminar failure prediction is obtained by using the equation

$$I = \left[(\sigma_z/F_z)^2 + (\tau_{xz}/F_s)^2 + (\tau_{yz}/F_s)^2\right]^{\frac{1}{2}}$$

where σ_z is the normal stress and τ_{xz} and τ_{yz} are the interlaminar shear stresses. Based on this normalization, any value of the interlaminar failure parameter greater than 1.0 could signify that failure occurs at the corresponding location.

The maximum interlaminar stress in the stringer flange occurs at the end of the flange, where it terminates at the intercostal flange, as shown in Fig. 6. At this location the interlaminar failure parameter

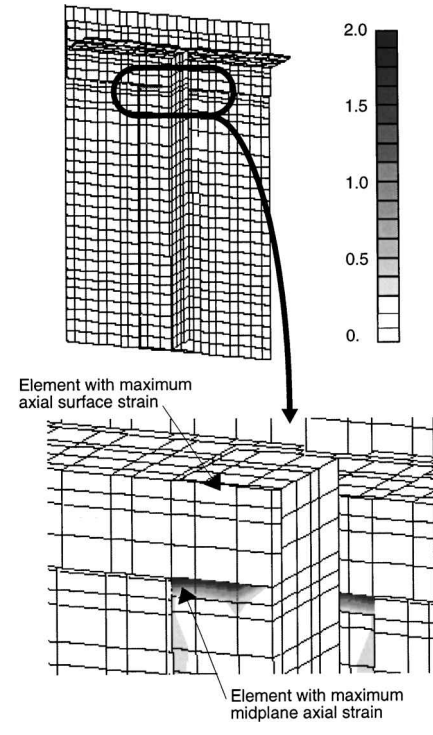

Fig. 6 Normalized stress at the skin–stringer flange interface for a load of 100,000 lb for the test panel.

is approximately equal to 2.0 for a load of 100,000 lb. Interlaminar strains at the ends of the panel, where the test specimen is surrounded by potting material, are not considered because delaminations are unlikely to occur inside the potting and would not propogate because of the support provided by the potting. Test results indicate that failure initiates at the interface between the skin and the stringer flange. The analytical prediction of the location of failure agrees with the experimental results. The panel failed at 99,200 lb of load.

Damage was inflicted to two locations of maximum axial strain in the skin on the unstiffened side of the test panel. These locations are near the termination of the stringer flange at the edge of the intercostal flange, as shown in Fig. 1. One impact was applied using a drop weight impactor and the other by using static indentation. A 1-in.-diam tup was used for impacts. The level of damage was defined by the amount of permanent indentation or dent depth. Both impacts to the test panel were approximately 0.15 in. deep. A dent that is more than 0.1 in. deep is assumed to be visible, and so these were considered severe damage. Damage occurred to the stiffened side due to impact to the unstiffened side.

The panel failed at a load of 94,600 lb through the impact sites. The allowable midplane strain assumed for damaged structure is 0.0053 in./in. The analysis of the undamaged structure predicts a strain at the impact site of 0.0053 in/in. for a load of 147,000 lb. Failure through the impact site would not be expected for loads less than 147,000 lb. Because the failure load is significantly less than 147,000 lb, the midplane strain at the impact site cannot be used to predict failure of this panel.

A method to predict failure in damaged, stitched graphite/epoxy structure by examining predicted bending and membrane strains a small distance away from the impact site is described in Ref. 6. This method calculates a so-called Potential Damaging Force (PDF) parameter that leads to a predicted failure load. In this method the midplane and surface strains for an undamaged structure are calculated. Failure would occur at the load resulting in the least surface and midplane strains that satisfy the following formula:

$$\frac{e_s - e_m}{e_{da}} + \frac{e_m}{e_d} = 1, \qquad e_{da} = \frac{e_d + e_u}{2}$$

where e_s is the axial surface strain, e_m is the axial midplane strain, e_d is the damaged allowable, and e_u is the undamaged allowable. Surface and midplane strains are calculated from finite element analysis of the undamaged structure. Allowable values are shown in Table 1.

A failure prediction for the damaged test panel based on this method results in a failure prediction of 95,550 lb. After being subjected to impact damage, the panel was loaded to failure. The panel failed at 94,600 lb of load, or 99% of the failure load predicted by using the method of Ref. 6. The bending behavior in the region of the impact site significantly influences the failure of the damaged panel. Additional test and analysis results are presented in Ref. 1.

In the test panels, the interlaminar strain between the stringer flange and the skin and the shear strain in the intercostal flange caused the failure of the undamaged panel. The axial strain near the impact site and the shear strain in the stringer flange caused the failure to occur in the damaged panel.

Thin-Skin Panel Parametric Study

The thin-skin panels were analyzed with simple supported unloaded edges using a nonlinear analysis for load up to 120,000 lb for comparison purposes. Typical cover panel analysis is limited to examining the maximum axial strain at the element midplane. For the parametric study, in addition to examining the axial midplane strain, the maximum in-plane shear strain at the element midplane and the maximum interlaminar shear stresses were examined. Because of differences in configurations, the locations of these maximum strains are not the same in every panel.

Using the midplane strain allowables and the interlaminar parameter defined in the preceding section, a maximum load can be determined for each panel for each of the three failure modes considered. A value of $I = 2$ is assumed to indicate failure because delamination began in the test panel at a load corresponding to approximately $I = 2$. These predicted failure loads are shown in Fig. 7 and Table 3. The failure prediction for each panel corresponds to the lowest failure load of the three modes. These predicted failure modes are shown in Table 4.

Table 3 Panel description

Configuration	Blade height	Blade thickness	Intercostal attachment
A	Constant	Tapered	Yes
B	Constant	Tapered	No
C	Constant	Constant	Yes
D	Tapered	Tapered	No
E	Tapered	Constant	No
F	Constant	Tapered	Yes

Table 4 Predicted failure modes of undamaged panels

Configuration	Thin skin (5-stack skin)	Thick skin (10-stack skin)
A[a]	Interlaminar	Shear
B	Interlaminar	Shear
C	Interlaminar	Interlaminar
D	Interlaminar	Interlaminar
E	Interlaminar	Interlaminar
F	Axial	Axial

[a]Configuration A with a thin skin corresponds to the test panel.

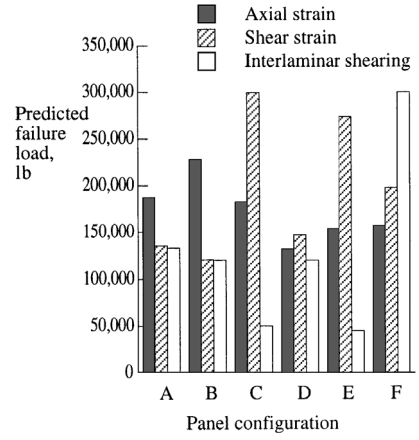

Fig. 7 Failure loads for undamaged thin-skin panels based on axial strain, shear strain, and interlaminar stress failure criteria; failure corresponds to the lowest failure load of the three modes. Configuration described in Table 3.

These results indicate that five panels (configurations A–E) would fail due to high interlaminar strains and that the other panel (configuration F) would fail due to high axial strains. This pattern of normalized interlaminar stress shown in Fig. 6 is typical of all panels that would fail due to high interlaminar stresses. The midplane axial strains for panel F subjected to a compressive load of 120,000 lb are shown in Fig. 8 with predicted failure location in the stringer flange. Only two configurations would be expected to support more than 120,000 lb. These panels are configuration A, with a constant-height and tapered-thickness blade, which would be expected to fail at a load of approximately 133,000 lb, and configuration F, which would fail at a load of approximately 157,000 lb. Configuration F is like configuration A except that the stringer flange continues under the intercostal flange in configuration F whereas it terminates without passing under the intercostal in configuration A. Panel A would support 84% of the load carried by panel F. By the running of the stringer flange under the intercostal flange, shearing in the blade and bending in the skin are reduced. By the reducing of bending, interlaminar forces are reduced, load-carrying capability is increased, and the failure mechanism is changed. The configuration that would support the least amount of load is configuration E, with a tapered-height, constant-thickness blade. Panel E is expected to fail at a load of 44,000 lb.

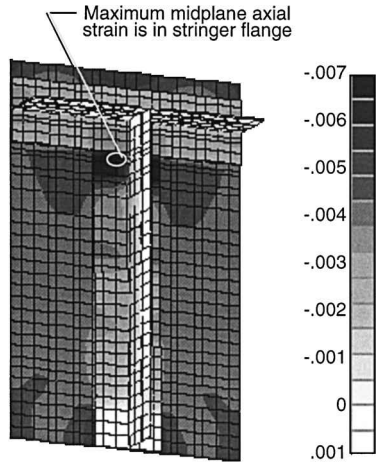

Fig. 8 Axial midplane strain in undamaged thin-skin panel F subjected to 120,000-lb load.

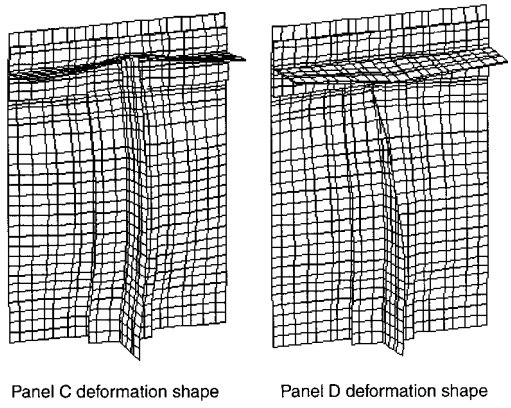

Fig. 9 Deformation of thin-skin panels C and D subjected to 120,000-lb load.

Because the load path is different in panels in which the stringer is connected to the intercostal from the path in panels in which the stringer is not connected to the intercostal, displacement patterns differ significantly. The displacement of panel C, with the constant-thickness, constant-height stringer, and of panel D, with the tapered-thickness, tapered height stringer, is shown in Fig. 9 for a load of 120,000 lb. This difference in displacement pattern induces differences in interlaminar stresses and bending strains.

The difference between the load levels at which failure is expected to occur due to interlaminar effects and due to high shear strains is less than 5% for both panels with constant-height and tapered-thickness blades (A and B). This observation indicates that either mode could cause failure in a test panel, and the initial failure mechanism would depend on small differences in panel construction.

The boundary conditions analytically imposed in the parametric study allow less bending to occur than the boundary conditions used in the panel test, so that bending behavior is less significant in the parametric study results than in the test panel.

Thick-Skin Panel Parametric Study

The thick-skin panels were analyzed with simple supported unloaded edges to a load of 450,000 lb for comparison purposes. For each panel, the maximum shear strain at the element midplane, the maximum axial strain at the element midplane, and the maximum interlaminar shear stresses were examined.

Using midplane strain allowables and the interlaminar failure prediction parameter I defined in the preceding section, a maximum load can be determined for each panel for each of the three failure modes considered. These loads are shown in Fig. 10 (see Table 3). The failure prediction for each thick-skin panel corresponds to the lowest failure load for the three modes, and the failure modes are

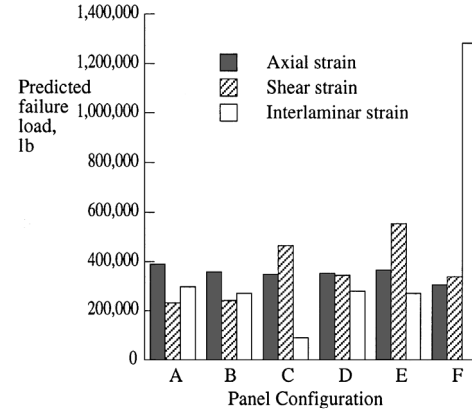

Fig. 10 Failure loads for undamaged thick-skin panels based on axial strain, shear strain, and interlaminar stress failure criteria; failure corresponds to the lowest failure load of the three modes. Configuration described in Table 3.

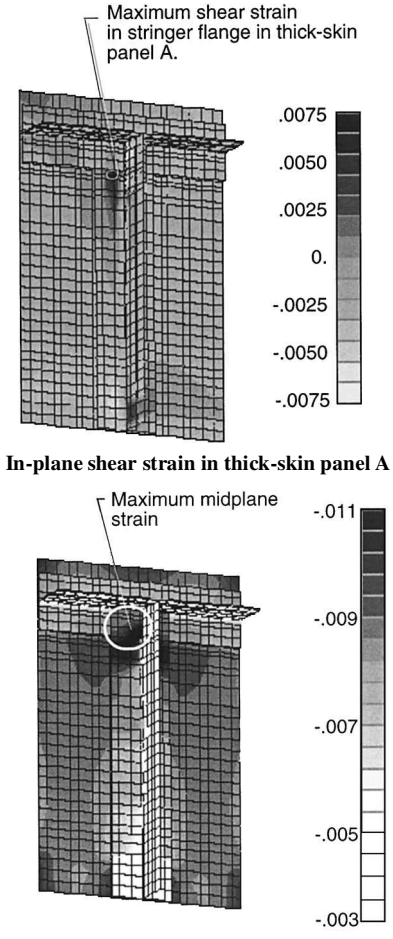

Fig. 11 Failure strain in undamaged thick-skin panels A and F subjected to 250,000-lb load.

shown in Table 4. These results indicate that panels A and B would fail due to high in-plane shear strains in the stringer flange, as shown in Fig. 11a for panel A. Panels C, D, and E would fail due to high interlaminar shear stresses with a pattern similar to that shown in Fig. 6. Panel F would fail due to high axial strain in the stringer flange in the extended region of the flange that is between the skin and the intercostal flange. The strain in this extended flange region is as shown in Fig. 11b by removing the intercostal flange elements

that would be on top the extended flange. The panel with the highest failure load is panel F, which has the longer flange, and would fail at a load of 308,770 lb. This extra flange length significantly reduces the interlaminar shear forces between the skin and stringer flange and reduces bending. It also decreases shearing in the blade and the flanges. The panel with the second highest failure load is panel D, which would fail at 281,000 lb. The configuration that would support the least amount of load is configuration C, with a constant-height, constant-thickness blade. Panel C is expected to fail at a load of 90,200 lb. Differences in load paths and deformation patterns as discussed for thin-skin panels effect the strains and, therefore, the failure loads of thick-skin panels as well.

Impact Damage Effects

Wing panels must be designed to tolerate a certain level of impact damage to the panel skin. Only skin elements are considered in this discussion of impact damage effects because the skin is the most likely location for the wing to sustain impact damage severe enough to reduce load-carrying capability. If panels were impacted, the allowable axial strain at the midplane would decrease from 0.0093 in./in. to 0.0053 in./in.

If the panel is impacted at a point where there is significant bending, the PDF parameter developed in Ref. 6 should be considered. Therefore, both the bending strains and the midplane strains must be considered. The location of the maximum midplane strain does not always coincide with the location of maximum bending strains. When applied to the thin-skin panels considered in the parametric study, the PDF parameter approach predicts failure loads that are less than those predicted by using only the allowable midplane strain for impact-damaged structure for all six configurations. When applied to the thick-skin panels, the PDF parameter approach predicts failure loads that are less than those predicted by using the impact-damaged allowable midplane strain for damaged structures for configurations A–D, but not for configurations E and F. Failure modes for thin- and thick-skin panels are shown in Table 5. Failure loads for impact-damaged thin- and thick-skin panels are shown in Figs. 12 and 13 (see Table 3), respectively.

The failure load of thin-skin panels is reduced by 0–65% because of impact damage. Panels A, B, D, and F would fail through the impact-damage site due to the effect of impact damage and bending, as indicated by the PDF parameter. Only the failure of panels C and E would be unaffected by impact damage because failure would be due to interlaminar shearing whether damage is present or not. The panel with the largest failure load is panel F, with a predicted failure load of 112,000 lb. Impact damage to panel F, reduces its failure load by 37%. The panel with the next largest failure load is panel A, with a predicted failure load of 82,000 lb. Panel A would fail at a load 27% less than the failure load of panel F. These results assume that

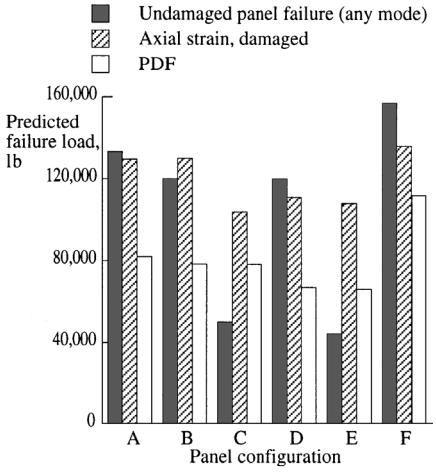

Fig. 12 Failure loads for impact-damaged, thin-skin panels based on axial strain, shear strain, and interlaminar stress failure criteria; failure corresponds to the lowest failure load of the three modes. Configuration described in Table 3.

Table 5 Predicted failure modes of impact-damaged panels

Configuration	Thin skin	Thick skin
A	Bending[a]	Bending[a]
B	Bending[a]	Bending[a]
C	Interlaminar	Interlaminar
D	Bending[a]	Bending[a]
E	Interlaminar	Axial
F	Bending[a]	Axial

[a]High axial surface and midplane strain at damage site.

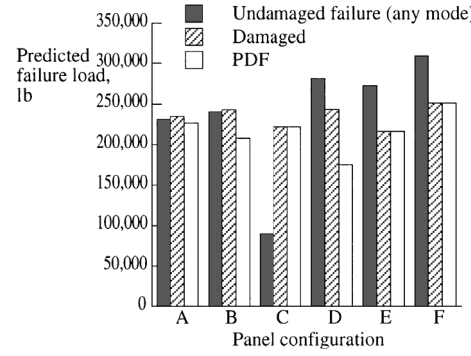

Fig. 13 Failure loads for impact-damaged, thick-skin panels based on axial strain, shear strain, and interlaminar stress failure criteria; failure corresponds to the lowest failure load of the three modes. Configuration described in Table 3.

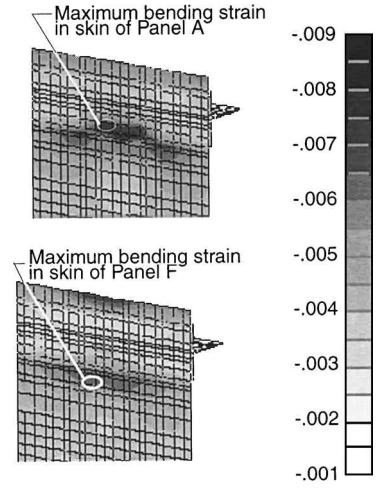

Fig. 14 Failure location for impact-damaged, thin-skin panels A and F.

the panel is impacted on the skin at the point of maximum bending of the skin, which is the most critical location. Axial surface strains in the skin and predicted failure locations for impact-damaged thin-skin panels A and F are shown in Fig. 14. Only skin runout regions are shown.

The failure load for thick-skin panels is reduced by 0–37% because of impact damage. Only the failure of panel C, with the constant-thickness, constant-height blade, is unaffected by impact damage because it would fail due to interlaminar shearing even with impact damage to the skin. All other thick-skin panels would fail through the impact site. Panels A, B, and D, all with tapered thickness, would fail due to the combination of high bending and impact damage, whereas panels E and F would fail due to excessive midplane strain at the impact site. The impact-damaged thick-skin panel with the highest failure load is panel F, with the additional length of stringer flange. This panel would fail at a load of 250,800 lb. The second highest failure load for a thick-skin panel is for panel A, which would fail at a load of 226,500 lb. The impact-damaged, thick-skin panel with the lowest failure load is panel C. The impact damage does not contribute to failure for panel C. Surface strain patterns for these panels are similar for those shown in earlier figures

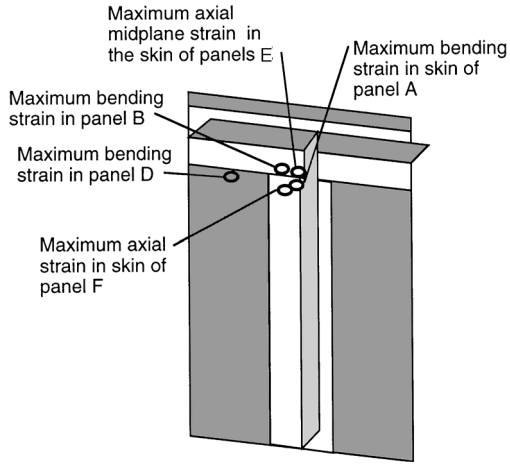

Fig. 15 Failure locations for impact-damaged, thick-skin panels A, B, D, E, and F.

so only predicted failure locations for thick-skin panels A, B, D, E, and F are shown in Fig. 15. Only skin elements are considered in danger of impact damage in this study, and so elements shown for panels A, B, E, and F are actually hidden by flanges.

Conclusions

Six configurations of graphite/epoxy panels with stringer terminations were evaluated for thin-skin and thick-skin panels. Three failure modes for undamaged panels were considered in the evaluation. Two additional failure criteria for impact-damaged panels were also used. The highest failure load for the undamaged panels and for the impact-damaged panels is the configuration with the stringer flange extending underneath the intercostal flange. All other undamaged thin-skin panels had high interlaminar strains that were suppressed by extending the length of the stringer flange underneath the intercostal. Bending plays a significant role in the failure of thin-skin panels for several configurations. For the configuration supporting the highest value of load, the thin-skin, impact-damaged panel could be expected to support a load that is 63% of the undamaged panel failure load. For the thick-skin undamaged panels, interlaminar shear, in-plane shear, and axial strain would all cause failure to occur in the panels with different configurations. The configuration with the stringer flange running under the intercostal flange would fail because of high axial strain in the impact-damaged and undamaged panels. The impact-damaged, thick-skin panels fail at a load that is 88% of the undamaged panels failure load. The failure mechanism is dependent on the stringer configuration. Interlaminar stresses and bending must be considered to predict the failure of thin-skin panels, and interlaminar, shear, and axial strains must be considered to predict the failure of thick-skin panels.

References

[1] Jegley, D. C., "Behavior of Compression-Loaded Composite Panels with Stringer Terminations and Impact Damage," *Journal of Aircraft*, Vol. 35, No. 6, 1998, pp. 942–948.

[2] Jegley, D. C., and Bush, H. G., "Structural Test Documentation and Results for the McDonnell Douglas All-Composite Wing Stub Box," NASA TM 110204, April 1997.

[3] Markus, A., Thrash, P., and Grossheim, B., "Manufacturing Development and Requirements for Stitched/RTM Wing Structure," NASA CP 3229, 1993, pp. 503–523.

[4] Brogan, F. A., Rankin, C. C., and Cabiness, H. D., "STAGS User Manual," Lockheed Missiles and Space Co., Palo Alto, CA, P032594, 1994.

[5] Brewer, J. C., and Lagace, P. A., "Quadratic Stress Criterion for Initiation of Delamination," *Journal of Composite Materials*, Vol. 22, Dec. 1988, pp. 1141–1155.

[6] Hinrichs, S., "General Methods for Determining Stitched Composite Material Stiffnesses and Allowable Strengths, Volume I," McDonnell Douglas Rept. MDC94K9113, Long Beach, CA, March 1995.